2015 IEEE/RSJ International Conference on Intelligent Robots and Systems (IROS)
Congress Center Hamburg
Sept 28 - Oct 2, 2015. Hamburg, Germany

A Micro Spherical Rolling and Flying Robot

Christopher J. Dudley, Alexander C. Woods and Kam K. Leang†

***Abstract*—This paper presents the design, fabrication, modeling, and demonstration of a micro spherical rolling and flying robot, with a total mass and payload of 35 g and 10 g, respectively. The micro aerial terrestrial robot (ATR) has the ability to fly through the air or roll on the ground, for applications that include search and rescue, mapping, and surveillance. Its unique size makes is easily portable and enables the robot to enter and maneuver around in tight spaces such as air ducts. The design centers around a micro-quadcopter encased in a lightweight spherical exoskeleton that can rotate about the quadcopter. The spherical exoskeleton offers agile ground locomotion while maintaining characteristics of a basic aerial robot in flying mode. Details of the system modeling, design and fabrication are discussed, including the robot's turning capabilities over ground and the lightweight spring-steel exoskeleton. The prototype ATR is experimentally validated in aerial and terrestrial mode, and results show that the ATR traveling over the same distance in rolling mode is 260 percent more efficient than a traditional flying-only robot and in flying mode the system is only 39 percent less efficient. Experimental results also demonstrate transition between modes of locomotion and curved, rolling trajectories.**

I. Introduction

AERIAL robots that can hover and maneuver quickly and accurately in tight urban and indoor spaces are well suited for applications that include search and rescue, mapping, surveillance, and environmental sensing [1], [2]. Interest in aerial robots has grown at a rapid pace, but relatively short flight time, limited control of maneuvers, self-localization, sensing, and safety pose significant challenges [2]. This paper focuses on the development of a micro robot (<50 g) that combines aerial and terrestrial (hybrid) locomotion to address the challenges of efficiency and limited functionality of aerial vehicles, as well as locomotion through environments such as tight spaces, channels, and air ducts.

Research and development of hybrid aerial terrestrial robotics is an active field. Many aerial terrestrial robots are composed of separate aerial and terrestrial actuators attached together to form a hybrid system. For example, the micro air-land vehicle (MALV) II is a fixed-wing propeller driven aerial vehicle with attached wheel-leg drive system for terrestrial locomotion [3]. A hexapedal winged robot equipped with flapping wings was developed to increase the overall running speed of a terrestrial robot [4], with future possibility of a fully functional flying and crawling robot. An ultra-light jumping and gliding robot capable of jumping 27 times its own height has been developed to mimic a desert locust [5]. In contrast, the proposed micro aerial terrestrial robot (ATR) uses the same actuators for both modes of locomotion, resulting in a lightweight and mechanically simple design. Recently, a hybrid quadcopter system was developed that translates downward thrust from the propellers into forward walking motion of legs [6]. A cylindrical quadcopter-based aerial-terrestrial robot that is capable of both efficient ground and aerial locomotion was recently developed [7]. Additionally, a fixed-wing aerial robot was recently developed that can move on the ground using its wings [8].

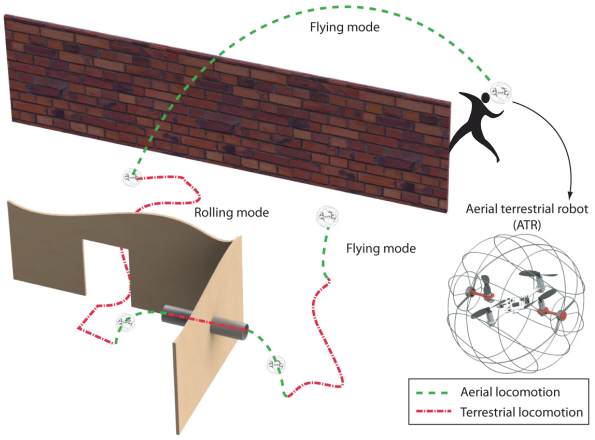

Fig. 1. Concept of the micro rolling and flying aerial terrestrial robot (ATR). The robot can be hand launched and operate in either flying or rolling mode. Rolling mode is convenient for energy efficient locomotion and maneuvering through tight spaces and challenging terrain.

The contribution of this work is the design, fabrication, modeling, and demonstration of a micro rolling and flying ATR, weighing less than 50 g. The micro ATR consists of an air-borne (e.g., multi-rotor) platform encased in a bearing driven spherical exoskeleton which can be exploited for energy efficient rolling without the use of any additional actuators, preserving the system's mechanical simplicity. Figure 1 shows the ATR concept and the various modes of locomotion. The prototype ATR consists of a micro quadcopter, axle, bearings, lightweight steel exoskeleton, and battery has a combined weight of 35.24 g and payload capacity of 10.36 g. Because the ATR is smaller than 6 inches (152 mm) in diameter, the user can easily hand launch the robot like a ball into flying mode, and depending on the situation, the robot can fly or enter rolling mode to traverse over the ground surface or through pipes and air ducts. Hybrid modes of locomotion enable the ATR to negotiate challenging obstacles and terrain while maintaining the benefits of each respective mode of locomotion. In addition to yawing about the ground contact point, a novelty of the ATR is its capability to turn while rolling in a method similar to how a railcar

†K. K. Leang (Corresponding author) is with the Design, Automation, Robotics, and Control (DARC) Lab, Department of Mechanical Engineering, University of Utah, USA. E-mail: kam.k.leang@utah.edu

navigates curves in its tracks. The ATR can position itself on varying diameter rings of its exoskeleton in contact with the ground while rolling, causing the platform to turn in a circular manner and allows the ATR to follow complex curved ground trajectories. Compared to flying, rolling mode can be used to avoid detection and since the ATR does not need to support its own weight in rolling mode, it can be more energy efficient, thus preserving battery power.

II. Design Overview

The basic design of the ATR is shown Figure 2(a). The system consists of a hover-capable flying robotic platform surrounded by an outer lightweight spherical exoskeleton and rotating supporting axle. The ATR's exoskeleton, when in terrestrial mode [Fig. 2(b)], rotates about the platform's central axis on its outer exoskeleton. The flat surface on either end of the axle creates a resting surface, as illustrated in Fig. 2(c). By orienting the ATR so that it sits on either side, the platform is able to rest in a stable position.

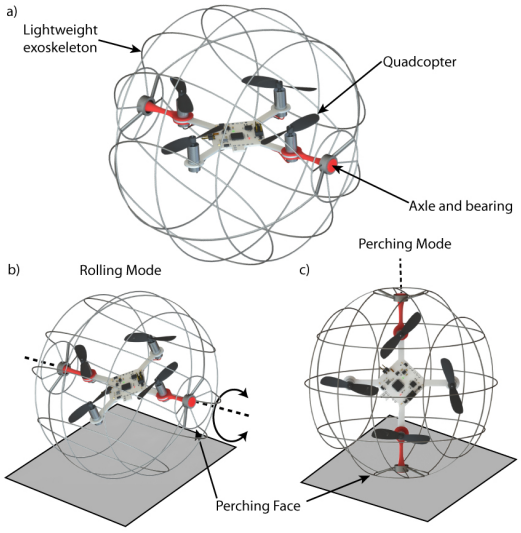

Fig. 2. Spherical-shaped aerial terrestrial robot: (a) key components, (b) rolling mode, and (c) perching mode.

The quadcopter platform used to create the ATR has a footprint of approximately 135 mm by 135 mm, measured along the platform arms from one rotor tip to the opposite rotor tip. The quadcopter and battery pack (1S1P 350 mAH lithium-polymer battery) weigh 28.7 g combined, and at full throttle, the quadcopter can lift an additional 16.9 g. The complete ATR concept, which consists of the quadcopter, axle, bearings, and lightweight steel exoskeleton, has a combined weight of 35.24 g and has a payload capacity of 10.36 g. Additional payload capacity can be achieved by design optimization and minimizing the weight of components and increasing the number or size of motors and rotors.

III. Modeling the ATR

Developing the governing equations of motion is an essential aspect for design and control of the ATR. The following section presents a model that captures the aerial and terrestrial locomotion of the ATR.

Let the inertial reference frame be denoted by $E \in \mathbb{R}^3$. The unit vectors: $\hat{e}_x$ is directed north, $\hat{e}_y$ is directed east, and $\hat{e}_z$ is directed to the center of Earth. The Earth's curvature is negligible for the scope of this work. An additional non-inertial, accelerating reference frame, B, fixed to the rigid body can be formed by $\hat{b}_x$, $\hat{b}_y$, $\hat{b}_z$, directed forward, right, and downward perpendicular to the body, respectively. A transformation exists to express a vector in either reference frame and can be represented in various methods including, Euler rotation angles, quaternion transformation, and angle-axis representation. The velocity of the rigid body can be represented in B and E as, $\vec{v}_{\{B\}} = \mathrm{a}\hat{b}_x$, $\vec{v}_{\{B\}} = \mathrm{c}\hat{e}_x + \mathrm{d}\hat{e}_x + \mathrm{f}\hat{e}_z$, where the subscript $\{B\}$ indicates the reference frame of interest. The Newton-Euler equations that fully describe the translational and rotational dynamics of the ATR are given by the following compact matrix representation,

$$\begin{bmatrix} \vec{f}_{\{B\}} \\ \vec{\tau}_{\{B\}} \end{bmatrix} = \begin{bmatrix} \mathbf{M} & \mathbf{0} \\ \mathbf{0} & \mathbf{I} \end{bmatrix} \begin{bmatrix} \dot{\vec{v}}_{cm_{\{B\}}} \\ \dot{\vec{\omega}}_{\{B\}} \end{bmatrix} + \begin{bmatrix} \vec{\omega}_{\{B\}} \times m\vec{v}_{cm_{\{B\}}} \\ \vec{\omega}_{\{B\}} \times I\vec{\omega}_{\{B\}} \end{bmatrix}, \quad (1)$$

where $\mathbf{M} \subset \mathbb{R}^{\mathbf{3}}$, $\mathbf{I} \subset \mathbb{R}^{\mathbf{3}}$are the mass and inertia matrix. The body's linear and angular accelerations $\dot{\vec{v}}_{cm_{\{B\}}}$, $\dot{\vec{\omega}}_{\{B\}}$, external forces, $\vec{f}_{\{B\}}$, and torques, $\vec{\tau}_{\{B\}}$, are defined in the body frame.

A. Aerial Locomotion

The quadcopter can be approximated as a rigid body with six degrees of freedom in the inertial frame. The position and attitude of the aircraft are given by $(\hat{e}_x, \hat{e}_y, \hat{e}_z)$ and $(\hat{\phi}, \hat{\theta}, \hat{\psi})$, respectively. The general Newton-Euler Equation (1) can

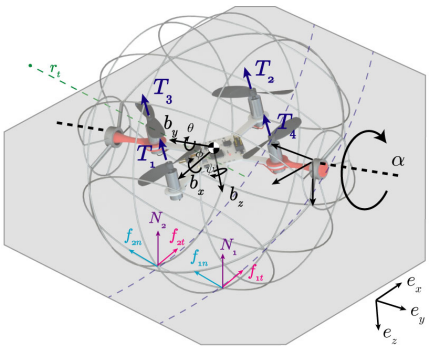

Fig. 3. The ATR system in terrestrial locomotion mode, powered by the brushed motors propelling and directing the rolling exoskeleton. The ATR is capable of smooth turning by positioning itself onto a set of its rings and rolling in a circular pattern.

be applied to the ATR flying platform with minor modification. First, it is assumed that the quadcopter platform is symmetric about the $\hat{b}_x$ and $\hat{b}_y$ axis, resulting in a symmetric and diagonal inertia matrix — no products of inertia exist, only three principle moments of inertia. The exoskeleton is assumed to be uniform in inertia about each principle axis, and only affects the inertia of the ATR system in the I_{yy} and I_{zz} direction as the bearing friction is much smaller in magnitude compared to the actuator action in aerial mode and the actuators do not have a direct impact on the rotation

of the exoskeleton in aerial mode. The motor thrust T_i and moment M_i are dependent on the motor torque and moment constants k_T, k_M which are a quadratic function of the rotor angular velocity Ω_i [9].

As shown in Fig. (3), the quadcopter can be represented in both the inertial reference frame, E, and the quadcopter rigid body frame B. Note that the linear and angular motions are coupled since the linear velocity in body coordinates depends on the current orientation. The dynamic equations of motion for the ATR in the body frame, B, are given by,

$$\ddot{z} = \sum_{k=1}^{4} \frac{T_i}{m} - g\hat{e}_z, \tag{2}$$

$$\ddot{\phi} = \frac{1}{I_{xx}}[k_T l(\Omega_4^2 - \Omega_3^2) + \dot{\theta}\dot{\psi}(I_{yy} - I_{zz}) + \sum_{k=1}^{4} J_r \Omega_k \dot{\theta} + I_{s_{zz}}\dot{\psi}\dot{\alpha}],$$

$$\ddot{\theta} = \frac{1}{I_{yy}}k_T l(\Omega_1^2 - \Omega_2^2) + \dot{\phi}\dot{\psi}(I_{zz} - I_{xx}) - \sum_{k=1}^{4} J_{r_k}\Omega_k\dot{\phi} + I_{s_{yy}}\ddot{\alpha}],$$

$$\ddot{\psi} = \frac{1}{I_{zz}}[k_M(\Omega_3^2 + \Omega_4^2 - \Omega_1^2 - \Omega_2^2) + \dot{\phi}\dot{\theta}(I_{xx} - I_{yy}) + \sum_{k=1}^{4} J_{r_k}\dot{\Omega}_k + I_{s_{xx}}\dot{\phi}\dot{\alpha}].$$

It is important to note that since the inertia of the exoskeleton and the inertia of the quadcopter platform are similar in magnitude, the rotation and inertia of the exoskeleton can greatly affect aerial locomotive dynamics. The addition of the exoskeleton does not increase the system inertia, $\mathbf{I}$, uniformly. The I_{yy} and I_{zz} terms nearly double, while I_{xx} remains only that of the quadcopter, resulting non-axisymmetric dynamics that are more difficult to control than traditional quadcopter systems. The lightweight exoskeleton with inertia $\mathbf{I_s}$, provides an additional torque on the ATR during flight if the exoskeleton is rotating after take-off at an angular velocity of $\dot{\alpha}\hat{b}_y$. Finally, it is noted that the effect of torques opposing the exoskeleton angular momentum is reduced by increasing $\dot{\alpha}$, which can contribute to the ATR's ability to maintain a desired heading in aerial mode.

B. Terrestrial Locomotion

Rolling forward or backward can be achieved by orienting the micro-quadcopter so that it provides a component of thrust along the horizontal direction (parallel to the ground). A novelty of the ATR is its capability to turn while rolling in a method similar to a railcar, where the ATR can position itself on its exoskeleton rings of varying diameter in contact with the ground, causing the platform to turn in a circular manner. Additionally, the ATR is capable of turning in place by creating a moment imbalance between motors, analogous to yaw action in aerial mode. Perching, as shown in Fig. 2 (c), allows the ATR to rest in a passively stable state and is accomplished by rotating the platform about its $\hat{b}_x$ axis by $\pm 90^\circ$ onto one of the flat ends of the sphere. These three configurations describe the gross behavior of the ATR over the ground.

1) Rolling: The dynamic equations presented in Eq. (2) apply specifically to aerial locomotion and can generally be applied to the terrestrial locomotion with some considerations. As shown in Fig. 3, the ATR must maintain a set-point pitch angle by increasing or decreasing the angular velocity of motors 1 and 2 to achieve a desired pitch angle, θ, resulting in a horizontal component of thrust for forward or reverse rolling motion. A vertical configuration with $\theta = \pm 90^\circ$ provides the most terrestrial thrust for rolling, but rotation about the $\hat{b}_x$ axis becomes more difficult to control as it relies solely on the moment produced by the motors, rather than the thrust, resulting in a possible loss of control. This configuration also decreases the robot's ability to roll about the $\hat{b}_x$ axis, limiting its ability to roll and turn simultaneously. For these reasons and the fact that small pitch angles $5^\circ < \theta < 10^\circ$ provide sufficient thrust for quick rolling locomotion at low overall thrust, an attitude constraint is formed that ensures the robot remains in contact with the ground, and is given by, $\sum_{k=1}^{4} k_T \Omega_i^2 \cos\theta \cos\phi < mg$.

The ground motion of the ATR is limited to rolling, sliding, or a combination of the two. Consider straight line motion of the ATR, transitioning from aerial locomotion to terrestrial locomotion with initial velocity, $\vec{v}_0$, thrust, $\vec{T}_x$, and initial angular velocity, $\dot{\vec{\alpha}}_0 = 0$. Upon ground impact, the acceleration of the mass center and angular acceleration of the sphere are,

$$\dot{\vec{v}}_{cm} = \frac{T_x}{m}\hat{e}_x - \mu_k g; \ddot{\vec{\alpha}} = \frac{\mu_k m g r_i}{I_{yy}}. \tag{3}$$

It is important to note that friction from the ground acts immediately, starting to slow the ATR down, bringing the exoskeleton into rotation. Pure rotation can only occur when, $\vec{v}_{cm} = r_i\dot{\vec{\alpha}}$, where r_i is the radius of the ring in contact with the ground and $\dot{\vec{\alpha}}$ is the angular velocity of the spherical exoskeleton. This relationship directly relates the rotation of the spherical exoskeleton and the linear velocity of the robot, forming a nonholonomic configuration constraint of pure rolling without slipping. Although a majority of the ATR's behavior follows the nonholonomic constraint, sliding and twisting motion must be considered during normal operation. From Eq. (3) and the nonholonomic constraint, the impact condition of rolling or sliding along the ground can be determined from the initial impact velocity, $\vec{v}_0$, thrust, $\vec{T}$, friction coefficient, μ_k, and contact radius, r_i.

The journal bearing used in the design exhibits a torque that opposes the rotation of the exoskeleton. This torque, τ_b, is primarily dependent on the contact surfaces, quadcopter platform mass, exoskeleton angular velocity, $\dot{\alpha}$, bearing temperature, and lubrication condition. An expression for the opposing torque due to bearing friction is given by, $\tau_b = mg\mu_b\frac{D}{2}\hat{b}_y$, where μ_b is the coefficient of rolling friction for the bearing and D is the bearing diameter. The μ_k can vary up to an order of magnitude over the life of the bearing, thus this must be taken into consideration.

2) Turning: The novelty of the ATR's maneuverability in terrestrial locomotion mode lies in the shape of the spherical exoskeleton. In addition to yawing the platform and spinning

about the $\hat{b}_z$ axis, the robot is geometrically designed to turn via varying diameter concentric rings, similar to how a solid axle train navigates turns on its track. An actuation imbalance between motors 3 and 4 and corresponding robot roll angle, ϕ, places the robot onto different sized sets of rings, and when the exoskeleton rolls, the robot turns in a circular manner due to the smaller and larger path of each contact ring. The platform turning radius, r_t, from the inner contact ring is given by,

$$r_t = \frac{r_2 q}{r_1 - r_2}, \tag{4}$$

where r_2, r_1 are the smaller and larger diameters of contact rings and q is the distance between rings as shown in Fig. 4. The ATR is equipped with three ring sets on either side of the robot, making complex turns of varying radius possible. The ATR can position itself on the proper set of rings by rotating about its $\hat{b}_x$ axis an amount,

$$\phi = \tan^{-1}\left(\frac{r_1 - r_2}{q}\right). \tag{5}$$

For simplicity in modeling the terrestrial rolling and turning, an additional reference frame is formed in the exoskeleton body frame. This frame is similar to the quadcopter body frame, but is not influenced by the rolling or pitching of the quadcopter and the $\hat{b}_{s_x}$ and $\hat{b}_{s_y}$ axes are coplanar with the $\hat{e}_x$ and $\hat{e}_y$ axes. The frame origin is at the mass center of the system (center of the sphere) and coincides with the quadcopter body frame. The forces and torques $T_{x,y,z}$, $\tau_{x,y,z}$ on the exoskeleton induced by the quadcopter actuators can be obtained from a simple transformation in a variety of methods outlined in III. Assuming both rings are in contact with the ground during turning, the forces and torques on the exoskeleton in the exoskeleton body frame are given as,

$$\ddot{x} = \frac{1}{m}[T_x - f_{1t} - f_{2t}], \tag{6}$$

$$\ddot{y} = \frac{1}{m}[T_y - f_{1n} - f_{2n}],$$

$$\ddot{z} = \frac{1}{m}[-T_z + mg - N_1 - N_2],$$

$$\ddot{\phi} = \frac{1}{I_{xx}}[\tau_x + r_1 f_1 n + r_2 f_2 n], \ddot{\alpha} = \frac{-1}{I_{s_{yy}}}[r_1 f_1 t + r_2 f_2 t + \tau_b],$$

$$I_{zz}\ddot{\psi} = \frac{1}{I_{zz}}[\tau_z + \frac{q}{2}(f_2 t - f_1 t)],$$

where f_{1t}, f_{2t}, f_{1n}, f_{2n} are the ring tangent and normal frictional forces as shown in Fig. 3, and N_1, N_2 are the normal forces in the $\hat{e}_z$ direction. The terms in Eq. (2) containing angular rates $\dot{\theta}$ and $\dot{\phi}$ are neglected in terrestrial analysis as the angular rates are minimal and do not appreciably impact terrestrial dynamics.

From Eq. (6) a relationship between the applied thrust, T_x, and the exoskeleton angular acceleration, $\ddot{\alpha}$, is given by,

$$\ddot{\alpha} = \frac{\tau_z + T_x q(r_2 - 0.5) - q\tau_b}{qI_{yy} + I_{zz}\frac{r_1+r_2}{2r_t+\frac{q}{2}} + mq(r_2 - 1)\left(\frac{r_1+r_2}{2}\right)}, \tag{7}$$

where r_1 and r_2 are the larger and smaller diameter rings of contact, q is the distance between rings, r_t is the turning radius, and τ_b is the bearing friction. The position and orientation of the exoskeleton are fully described by the rotation of the exoskeleton, α, and are parameterized in cartesian coordinates by,

$$x = x_0 + r_t \sin\left(\frac{\alpha(r_1 + r_2)}{2r_t + \frac{q}{2}}\right), \tag{8}$$

$$y = y_0 - r_t + r_t \cos\left(\frac{\alpha(r_1 + r_2)}{2r_t + \frac{q}{2}}\right),\ \psi = \frac{\alpha(r_1 + r_2)}{2r_t + \frac{q}{2}}.$$

Equations (6), (7), and (8), describe the motion of the ATR when turning in terrestrial mode.

Assuming the ATR has small inertia and can instantaneously change its roll angle, ϕ, complex paths can be achieved by varying the ATR's turn radius from each ring during rotation of the exoskeleton. An additional method for turning is accomplished by actuation of motor pairs 1 and 2, or 3 and 4, creating a net moment about the $\hat{b}_z$ axis that causes the robot to pivot about its point of contact on the ground. This action, combined with the geometric constraint in Eqs. (4), (5), (6), and (8) allow the designer to optimize the robot design for complex ground maneuvers that require minimal effort.

3) Resting Mode: The ATR is able to achieve a stable resting position from any arbitrary orientation by rotating about its center of mass to land on a resting surface located on either side of the robot. The onboard inertial measurement unit provides attitude measurement, and a setpoint of $\phi = \pm 90°$ is achievable by creating a net moment from an actuation imbalance of motor pair 3 and 4. Additionally, actuating a single motor to provide sufficient thrust can position the ATR in rest mode provided the moment provided by the motor, k_M, is not too large to affect rotation about another axis. The ATR can also be equipped with a grasping mechanism in the hollow axle that enables the robot to grip onto vertical surfaces like netting, textiles, or even small tree branches in future designs. This mechanism could possibly be actuated with a shape memory alloy, and due to the ATR's small mass, need not be extremely sizable.

IV. Robot Design

A. Quadcopter Platform Design

The body of the quadcopter is fabricated from a single printed circuit board and carbon fiber arms (4.5 g) which significantly reduces the overall mass, with surface-mount components that include a microcontroller (ATmega328P), a three-axis gyro and accelerometer (InvenSense MPU-6050) that fuses raw accelerometer and gyroscope data to report the attitude angles, ϕ, θ, ψ, at 100 Hz for attitude stabilization in both modes of locomotion, and MOSFET's for motor speed control. The platform is equipped with an XBee 2.4 GHz radio receiver for communication with a ground control station, and four small (7 mm x 17 mm) coreless brushed DC motors paired to 45 mm propellers. The system is powered with at 9.35 g, 350mAh Lithium-Polymer battery. Compared to larger quadcopter systems where brushless motors are

commonly used, brushed DC motors do not require sophisticated electronic speed controllers, further reducing weight. However, the trade off in this case is longevity, as brushed motors tend to wear more quickly during use compared to brushless motors.

The programming interface is a Serial Peripheral Interface (SPI) and enables the user to upload custom control software. Two way wireless communication between the platform and ground control station (GCS) is through a custom developed graphic user interface and Microsoft Xbox controller. Various buttons on the controller are used for pre-programmed autonomous flight, and the analog joysticks can be used for manual user input. A wireless link between the quadcopter and the GCS makes on-the-fly controller tuning and remote monitoring of attitude, control effort, and remaining flight time possible.

B. Exoskeleton Design

The ATR is able to conserve considerable power in rolling mode compared to conventional multirotor flying platforms. In previous work [7], the added mass of a protective cage was minimal in comparison to the overall capability of the robot, but the added mass of the ATR's spherical exoskeleton is similar in magnitude to the mass of the quadcopter, and must be considered for efficiency purposes and impact on system dynamics as outlined in III. The spherical exoskeleton was chosen to fit tightly around the quadcopter platform to minimize mass and enable the robot to be easily hand launched and capable of maneuvering through tight indoor spaces. While a diameter of 135 mm fulfills the design requirements, a larger sphere diameter of 152 mm (6 in) was chosen to protect the inner quadcopter and allow for compliance of the sphere when bouncing or falling from heights.

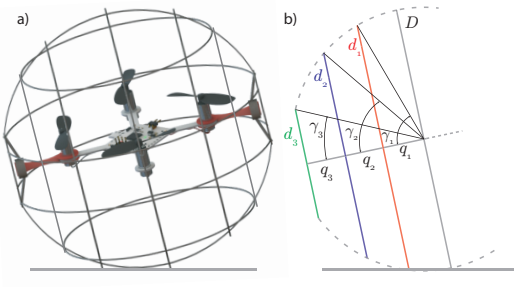

Fig. 4. Spherical exoskeleton design: (a) mode of operation, (b) design geometry with design parameters d_1, d_2, d_3 for varying γ.

Each ring diameter is constrained by the overall sphere diameter, D, and can be designed for a desired turn radius, r_t from the design angle, γ, as,

$$r_t(\gamma_1, \gamma_2) = \frac{\sin\gamma_2(\cos\gamma_2 - \cos\gamma_1)}{\sin\gamma_1 - \sin\gamma_2}. \tag{9}$$

The angle, γ, is measured from the $\hat{b}_y$ axis to the intersection of the ring diameter d_n with the sphere, as shown in Fig. 4(b) and completely defines the turn radii when accompanied by the diameter of the sphere, D. The designer is given freedom to choose γ_1, γ_2, and γ_n to achieve various discrete turn radii depending on which pair of rings the ATR rolls. For example, a larger diameter ring can be used for long, sweeping maneuvers and smooth transition to straight rolling or a smaller diameter ring can be used to maneuver in tighter constrained spaces. A range of possible d_1 is chosen to give a turn radius 32 cm$<$ r_{t1} $<$48 cm, and from the resulting range of d_1 values and Eq. (9), the designer can determine proper ranges for d_2, and d_3 to satisfy turning requirements. For this design, $r_{t1} = 32.1$ cm $r_{t2} = 17$ cm, and $r_{t3} = 6$ cm were chosen to give a suitable range of possible turning radii. It is important to note that the diameter of each ring influences the overall mass of the exoskeleton quadratically by, $m_n = \frac{\rho_w \pi^2 d_n^2 d_w}{4}$, where ρ_w and d_w are the ring material density and diameter, d_n is the ring diameter, and m_n is the ring mass. The designer must take care to design an exoskeleton that meets both the terrestrial maneuverability requirements while still satisfying the requirements for aerial flight. Due to extreme payload limitations of approximately 17 g, the exoskeleton was designed to be as light as possible, while still allowing the ATR to fall and tumble from heights. Additionally, the steel exoskeleton was designed with a degree of compliance that allows elastic deformation of the cage during impact, preventing damage to the robot. Various materials were considered to fulfill the design requirements, such as: 3D Printed Polylactic Acid (PLA), carbon fiber composite, titanium wire, and various diameters of spring steel wire. The difficulty in joining materials like titanium and complex molds for composite fabrication prevented quick design iteration, and ultimately, 0.020" diameter spring steel wire was chosen for the design due to its relatively easy workability and resulting lightweight exoskeleton (5.33 g as built). It is noted that these alternate materials can yield a lighter weight exoskeleton, but the steel wire design satisfies payload restrictions outlined in Section VI.

C. Control System

The focus of controller synthesis for the ATR is stabilization of each orientation angle ϕ, θ, ψ. Once the attitude of the robot is controlled, higher level position controllers can be implemented for rate control, object avoidance, and trajectory tracking with the use of additional sensors such as motion capture systems [10], optic flow [11], and LIDAR [12]. The control architecture consists of an inertial measurement unit sensor and cascaded discrete PID controller operating at 100 Hz. A base throttle command is used to control the ATR's z height in open loop. Each controller effort for the respective orientation angles is either added or subtracted from the respective motor. A simulation of the system dynamics in closed loop is used to estimate initial gains K_p, K_i, and K_d for each axis. It is noted that the model does not address aerodynamic effects such as propeller wash, drag, and rotor dynamics, which are known to have an impact on overall system performance [13]. The final controller gains are $K_p = 0.26$, $K_i = 0.12$, and $K_d = 0.04$.

D. Characterization

A custom test stand was fabricated to characterize the thrust, power consumed, current draw, and battery voltage as a function of motor angular velocity. The thrust and moment are characterized on 6-axis force and torque transducer (ATI Industrial Automation Nano17) over the full range of throttle inputs and can be used to determine the motor thrust constant, k_T and motor moment constant, k_M, shown in Fig. 5. The system inertias, masses, and physical parameters such as arm length and center of mass are estimated using a reliable SolidWorks model and high-precision scale and are reported in Table I.

TABLE I
ATR SYSTEM PARAMETERS

System Parameter	Value
Micro-quadcopter mass	26.31 g
Spherical exoskeleton mass	4.65 g
Micro-quadcopter inertia	[11944, 11998, 22480] g·mm^2
Spherical exoskeleton inertia	[17760, 16476, 17760] g·mm^2
Rotor inertia	21.35 g·mm^2
Micro-quadcopter arm length, l	40 mm
Motor thrust constant, k_T	1.761x10^{-8} $\frac{\text{N·s}}{\text{rad}}$
Motor moment constant, k_M	1.873x10^{-10} $\frac{\text{N·m·s}}{\text{rad}}$
Exoskeleton ring radii $[r_{1,2,3,4}]$	[75.0,68.6,44.8,16.5]
Exoskeleton ring spacing, q	30 mm
Bearing shaft diameter, D	0.125 in
Coefficient of bearing friction, μ_b	0.15

V. Simulation

Upon developing the governing equations of motion, the system is simulated in MATLAB Simulink to validate the model with experimental data and generate open-loop trajectories suitable for each mode of transportation. For example, a path for complex terrestrial locomotion such as rolling around obstacles, flying into a constrained space, and then continuing aerial flight can be simulated and each of the four motor commands can be recorded for future work. Additionally, various paths can be examined to determine the most efficient trajectory to reach a desired location.

VI. Fabrication

The exoskeleton of the ATR is fabricated from 0.020" diameter steel spring wire. The 6 inch form shown in Fig. 7(a) is inscribed with grooves used for aligning the concentric and orthogonal wire rings and ensures that the finished ATR is perfectly spherical for smooth terrestrial locomotion. After constructing the mold, wire bands were sized on the mold, abraded to remove surface contamination, cleaned with a solvent, and then soldered to create a loop as shown in Fig. 7(b). The soldered joint is then tightly wrapped with strands of thin copper wire to improve the joint integrity. The completed sphere halves shown in Fig. 7(c) are joined at the central ring of the right half, completing the exoskeleton. The quadcopter mass center was designed to coincide with the rotation axle of the ATR for balanced rotation about the $\hat{b}_y$ axis and a neutral inactive position. In previous work, a similar design includes a mass center offset that guarantees stability at rest [7], but since the inertia of the quadcopter used for the ATR is small compared to the motor pitching moment, the ATR quadcopter can be easily righted at the beginning of operation from any orientation. The axle is designed to be as light as possible while firmly grasping the quadcopter fuselage and is constructed with a 1/8 in hollow carbon fiber shaft fixed to the exoskeleton. The quadcopter is then affixed to an acetal journal bearing that extends the diameter of the exoskeleton, improving rigidity [Fig. 7(d)].

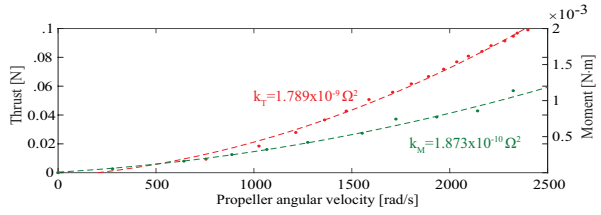

Fig. 5. a) Quadratic motor thrust and moment constant characterization.

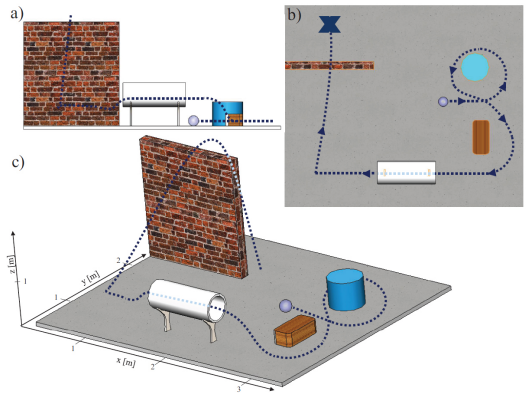

Fig. 6. Simulation of rolling and flying dynamics through a complex path.

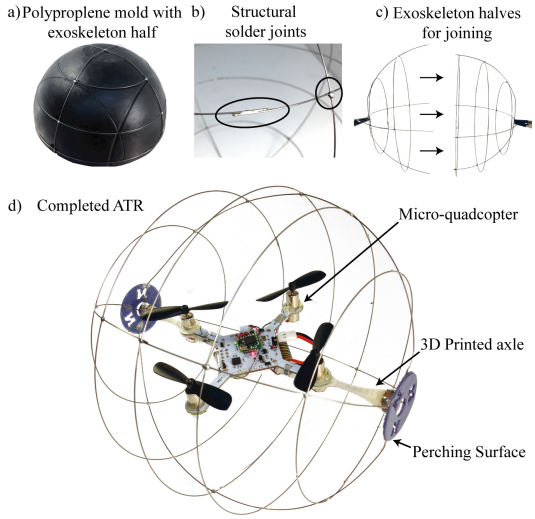

Fig. 7. Fabrication of the spherical exoskeleton: (a) completed half sphere on polyproplene mold, (b) structural solder joining the structure, (c) combining of completed half spheres, and (d) completed ATR with carbon fiber axle, low-friction journal and micro-quadcopter.

VII. Experimental Results and Discussion

The fabricated ATR was evaluated in an indoor environment with foam ground and netted walls to protect the ATR from impact. The aerial locomotion operates with approximately 75 percent throttle and 15.2 W of power necessary for hover, leaving sufficient throttle for maneuvers and stabilization control. The ground locomotion was tested and required approximately 20 percent throttle and 4.8 W of power.

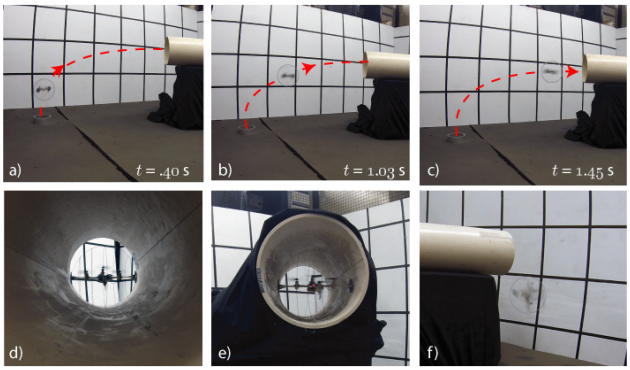

Fig. 8. Flying behavior of the ATR into a tube, then rolling through the tube and out.

The ATR was also tested in a practical environment, shown in Fig. 8, where the robot flew and entered a 7 inch diameter tube, rolled through, and exited. Transition from ground to aerial locomotion was also tested and is shown in Fig. 9. During experimentation, it was noted that stable hover upon take-off required a large control effort to combat the angular momentum from the spinning exoskeleton.

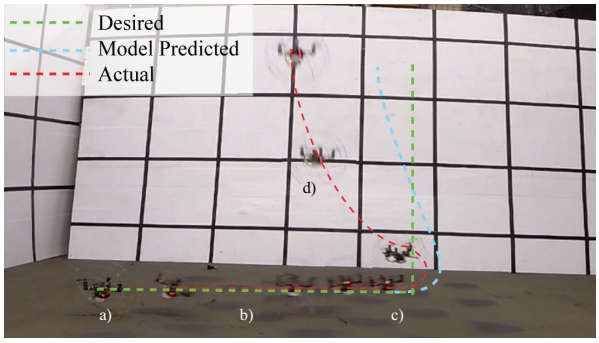

Fig. 9. Rolling to flying behavior of the ATR: (a) passive ATR position, (b), (c) transition to flight, and (d) flying mode.

To experimentally validate the increased efficiency of the ATR, the throttle position required to roll and fly in a straight line was measured for a set distance and the time was recorded. From the platform characterization in Section IV-D, and translational velocity, the time and distance to exhaust a 350 mAh battery was calculated for each respective mode. In rolling mode, the ATR can travel at 2.46 m/s with a current demand of 1.73 A and has a range of 1.79 km for 12.14 min. Comparatively, in flying mode, the ATR travels at 1.62 m/s with a current demand of 4.35 A and has a range of 469 m for 4.82 min, showing that the ATR's rolling mode is 3.66 times more efficient than flying mode. For the same aerial velocity, an unmodified quadcopter, weighing 28.2 g, can travel 652 m for 6.71 min, which is 39 percent more efficient than the ATR in flying mode, but the ATR's rolling mode is 2.63 times more efficient than the unmodified flying-only platform.

VIII. Conclusions and Acknowledgements

The design of a spherical aerial terrestrial robot was presented. The ATR has the ability to fly through the air or roll on the ground, for various applications from search and rescue to entertainment. It was estimated that the ATR can roll along the ground for over 12 minutes and cover the distance of 1.7 km, or it can fly for 4.82 minutes and travel 469 m, on a single 350 mAh battery. Compared to a traditional flying-only robot, the ATR in rolling mode is 263 percent more efficient, and in flying mode is only 39 percent less efficient. The ATR can transition seamlessly between operation modes and is capable of navigating through constrained spaces.

This material is based, in part, upon work supported by the National Science Foundation, Partnership for Innovation Program, Grant No. 1430328. Any opinions, findings, and conclusions or recommendations expressed in this material are those of the author(s) and do not necessarily reflect the views of the National Science Foundation.

References

[1] C. Luo, A. Espinosa, D. Pranantha, and A. De Gloria, "Multi-robot search and rescue team," in *Safety, Security, and Rescue Robotics (SSRR), 2011 IEEE International Symposium on*, 2011, pp. 296–301.

[2] V. Kumar and N. Michael, "Opportunities and challenges with autonomous micro aerial vehicles," *Int. J. of Robotics Research*, vol. 31, no. 11, pp. 1279 – 1291, 2012.

[3] R. J. Bachmann, R. Vaidyanathan, and R. D. Quinn, "Drive train design enabling locomotion transition of a small hybrid air-land vehicle," in *Intelligent Robots and Systems, IROS 2009. IEEE/RSJ International Conference on*, 2009, Conference Proceedings, pp. 5647–5652.

[4] K. Peterson, P. Birkmeyer, R. Dudley, and R. Fearing, "A wing-assisted running robot and implications for avian flight evolution," *Bioinspiration & Biomimetics*, vol. 6, no. 4, p. 046008, 2011.

[5] M. Kovac, J.-C. Zufferey, and D. Floreano, "Towards a self-deploying and gliding robot," *Flying insects and robots*, p. 271, 2009.

[6] A. Kalantari and M. Spenko, "Design and manufacturing of a walking quadrotor aerial vehicle," in *ASME International Design Engineering Technical Conference*, 2012, pp. 1067–1072.

[7] ——, "Design and experimental validation of hytaq, a hybrid terrestrial and aerial quadrotor," in *Robotics and Automation (ICRA), 2013 IEEE International Conference on*, 2013, Conference Proceedings, pp. 4445–4450.

[8] L. Daler, J. Lecoeur, P. B. Hahlen, and D. Floreano, "A flying robot with adaptive morphology for multi-modal locomotion," in *IEEE/RSJ International Conference on Intelligent Robots and Systems*, 2013.

[9] D. Mellinger, M. Shomin, and V. Kumar, "Control of quadrotors for robust perching and landing," in *Proc. Int. Powered Lift Conf*, 2010, pp. 119–126.

[10] D. Mellinger, N. Michael, and V. Kumar, "Trajectory generation and control for precise aggressive maneuvers with quadrotors," *The International Journal of Robotics Research*, vol. 31, no. 5, pp. 664–674, 2012.

[11] S. Zingg, D. Scaramuzza, S. Weiss, and R. Siegwart, "Mav navigation through indoor corridors using optical flow," in *Robotics and Automation (ICRA), 2010 IEEE International Conference on*. IEEE, 2010, pp. 3361–3368.

[12] S. Grzonka, G. Grisetti, and W. Burgard, "A fully autonomous indoor quadrotor," *Robotics, IEEE Transactions on*, vol. 28, no. 1, pp. 90–100, 2012.

[13] S. Bouabdallah, P. Murrieri, and R. Siegwart, "Design and control of an indoor micro quadrotor," in *Robotics and Automation, 2004. Proceedings. ICRA'04. 2004 IEEE International Conference on*, vol. 5. IEEE, 2004, Conference Proceedings, pp. 4393–4398.